PHYSICAL REVIEW A VOLUME 37, NUMBER 12 JUNE 15, 1988

Dynamical states and bifurcations of a thermal lens using spectral analysis

G. Gouesbet and E. Lefort
Laboratoire d'Energétique des Systèmes et Procédés,
Institut National des Sciences Appliquées (INSA) de Rouen, 76130 Mont Saint-Aignan, France
(Received 24 July 1987; revised manuscript received 1 February 1988)

Dynamical states and bifurcations of a thermal lens are studied with use of spectral analysis. The following dynamical states are observed: steady, periodic, quasiperiodic with two fundamental frequencies, and subharmonic states. Hysteresis is observed in the transition between periodic and quasiperiodic oscillations. Although chaos is not observed in the present work, thermal-lens oscillations can also lead to chaos as previously published. The control parameters are the laser power P and a distance d. The boundaries of the different dynamical states are given in the plane (P,d). Properties of the different dynamical states and of the transitions between states are studied.

I. INTRODUCTION

In recent years the transition to chaos in dissipative dynamical systems has received increasing interest with many important contributions, both theoretical and experimental. A good review is given by Eckmann[1] and also, more recently, by Cvitanović.[2] A recent comprehensive book by Bergé *et al.*[3] provides an overview of the involved concepts.

Several routes to chaos have been modeled and discussed by theorists. The most celebrated are probably the Ruelle-Takens scenario, where a strange attractor is likely to appear after three successive bifurcations,[4,5] the transition through an infinite cascade of subharmonic bifurcations,[6–8] and the intermittency model.[9–11] These routes and other connected phenomena have been experimentally observed and discussed in Refs. 12–17, a list which is very far from being exhaustive, although limited to early papers.

Another oscillatory phenomenon (thermal-lens oscillations) has been observed in our laboratory, exhibiting dynamical states of very rich behaviors. A research program has been undertaken to understand and describe this phenomenon. One part of this program has been devoted to the description of the dynamical states and bifurcations exhibited by the system when control parameters are modified. The present paper reports on the results obtained in this framework during the last few years.

II. GENERAL PRESENTATION OF THERMAL-LENS OSCILLATIONS

A. Thermal lensing and thermal-lens oscillations

The original observations are as follows.[18] A cw laser beam (Ar ion) is focused on a cell containing a ferrofluid (cobalt particles, 12 nm diameter, in toluene). When leaving the cell, the beam exhibits a strong divergence, with production on a screen of a regular and very-well-contrasted ring pattern. These phenomena have a thermal origin and can be interpreted as caused by the production of a thermal lens in the liquid. Thermal lensing has been studied in various situations in Refs. 19–25, among others. Furthermore, under certain conditions, when the laser beam travels horizontally just below the free surface of the liquid (or also vertically upwards), the ring pattern can depart from steadiness and exhibit various unsteady behaviors (periodic, quasiperiodic, chaotic). The oscillatory images produced by observing the outgoing beam on a screen have been given the name of optical "heartbeats," HB1 for an horizontal beam and HB2 for a vertical beam.[26] Only the HB1 is discussed in the present paper because dynamical states observed up to now with the HB2 have not been as rich as for the HB1.

Dynamical states depend on the nature of the liquid (included its absorbance for the illuminating wavelength), the cell geometry, boundary conditions such as ambient temperature and pressure, all the illuminating conditions among which we select the laser power P, and the distance d between the laser axis and the free surface. In the present paper everything is fixed but two control parameters: power P and distance d.

Bifurcation critical quantities depend very much on the liquid. For the onset of oscillatory behavior, the required power varies from 1 W for a "chromic acid cleaning mixture" ($CrO_3 + H_2SO_4$), to 100 mW or so for cobalt particles dispersed in toluene (ferrofluids), down to 10 mW for organic solvents colored with a dye (benzene, acetone, toluene, carbon tetrachloride). Oscillations have never been observed for some liquids, such as (colored) water. Our effort to produce thermal-lens oscillations at low laser powers is discussed in Ref. 27. Preliminary measurements have shown that the critical quantities for the onset of oscillations depend very much on the external temperature in the case of thermal-lens oscillations at small laser powers. For instance, critical frequencies are modified by 100% for an ambient temperature modification equal to 1 K. The present paper is consequently devoted to high laser power thermal lensing.

B. Present understanding of the instability mechanisms

Two directions for research have been explored. The first one concerns the understanding of the instability mechanisms leading to thermal-lens oscillations (HBE: optical heartbeat experiments). Using optical visualization techniques, it has been established that the optical heartbeats are accompanied by convective oscillations in the liquid bulk and surface oscillations at the free surface. These oscillations can also be produced when heating below the surface is carried out by means of a hot wire instead of a laser beam (HWE: hot-wire experiments). Critical temperature differences (between the hot-wire and the ambient temperature) and critical frequencies for the onset of oscillatory motion have been systematically measured, for four Rhodorsil silicon oils of well-known thermophysical properties.[27–30] A theoretical effort has been undertaken aiming at the prediction of the experimental critical quantities, first by using a purely numerical approach,[31] and secondly by examining the link between the HWE problem and overstability produced in a horizontal liquid layer destabilized simultaneously by buoyancy and surface tension agencies.[32,33] There are two important differences between the HWE and the HBE. For the first one, we note that heating is along a line in the HWE while it is nearly localized at a point in the HBE. In effect, in the HBE the divergence of the laser beam in the cell is produced in a very small region having a length which is much smaller than 1 mm. The second difference is as follows. In the HWE the hot wire is temperature controlled and the heating boundary conditions do not depend on the dynamical state of the system. Conversely, in the HBE there is a feedback between the heating conditions and the liquid motion, making thermal-lens oscillations a more complex phenomenon than the HWE. The absence of such a feedback in the HWE is probably the reason why, for these experiments, complex dynamical states have not been observed up to now, but merely the first transition from the steady state to the oscillatory state with a basic single fundamental frequency. However, from the knowledge gained by the aforementioned investigations and also from optical visualizations in the HBE, thermal-lens oscillations can be qualitatively described by the very simple sequence of events listed below.

At the entrance point of the converging laser beam in the cell, absorption produces an intense local heating which is spread, essentially by conduction, to the surrounding liquid. A thermal plume is then generated which is buoyancy driven up to the free surface in a convection-dominated regime. When the thermal plume reaches the free surface, it is disrupted by the Marangoni effect which drives the hot liquid toward the lateral boundaries of the cell (we assume that the derivative of the surface tension with respect to the temperature is negative, as usual). The liquid in the cell is then moved, driving a cold liquid at the laser beam location, and ending a cycle of the process. A new cycle is ready to start. The oscillatory behavior would then be linked to a continuous disruption and creation of thermal plumes. Actually, the different steps in the oscillatory process are coupled. They develop more simultaneously than sequentially. Two time scales must be associated with the above scenario: a buoyancy or Rayleigh time corresponding to the ascension of the thermal plume, and a surface tension or Marangoni time corresponding to its disruption at the free surface, the latter being usually much smaller than the first. The evolution of the HB is linked to this hydrodynamic scenario, the divergence of the outgoing beam being greater when the temperature gradients in the laser impact zone are larger. When the thermal plume is created, the HB dimensions increase progressively up to a maximum. The ascension of the thermal plume is accompanied by a weak decrease in the HB dimensions. The disruption produced by the Marangoni effect finally leads to a sudden contraction of the ring pattern on the screen.

The present paper is mainly devoted to a second direction of research, namely, to characterize dynamical states and bifurcations in thermal-lens behaviors when the two control parameters P and d are modified. Chaos has not been observed in the present series of experiments, although other experimental conditions can lead to it.[26,27]

III. THE EXPERIMENTAL SETUP

A. Presentation of the setup

The experimental setup is shown in Fig. 1. The source is a model 164 Spectra-Physics Ar-ion laser (item 1) working in the TEM_{00} mode at 514.5 nm, with an electric field vibrating in the vertical plane, and a beam diameter equal to 1.5 mm at $1/e^2$. Items 3 and 5 are two right-angle prisms, mounted on supports for adjustments with respect to three independent rotation angles, permitting them to produce a beam parallel to the laser output and then to increase the compactness of the experiments. Items 2 (a polarization rotator) and 4 (a fixed Glan prism) enable an accurate adjustment of the laser power. The laser beam is focused on to the internal entry face of the cell by a lens 6 (focal length = 150 mm).

Pellicle beam splitter 7 (8 μ thickness, transmission = 92%) reflects a part of the laser power to the set 13 (beam attenuator), 14 (photodiode, Hamamatsu, S1227, 1010 BR), and 15 (numerical voltmeter, with a charge resistance). This set permits a measurement of the laser power fed to the cell via a prior calibration using a laser powermeter. The beam attenuator is used to keep the photodiode 14 in a linear range of operation. The relative accuracy on P is estimated to be 5%.

The sealed cell 8 is a spectroscopy cell. Its vertical location is adjusted with an accuracy equal to 0.01 mm. The thickness 1 of the cell (that is to say, the thickness of liquid parallel to the laser beam-) can be 1, 2, 5, or 10 mm. The cell dimension perpendicular to the laser beam is $L = 10$ mm. The height is $H = 45$ mm. The height h of the liquid in the cell varies between 30 and 40 mm.

Screen 9 is a translucent one (Microcontrole, Marata 85-85, S390 023) permitting the visual observation of the HB. It is located 4 cm after the cell. It plays a second,

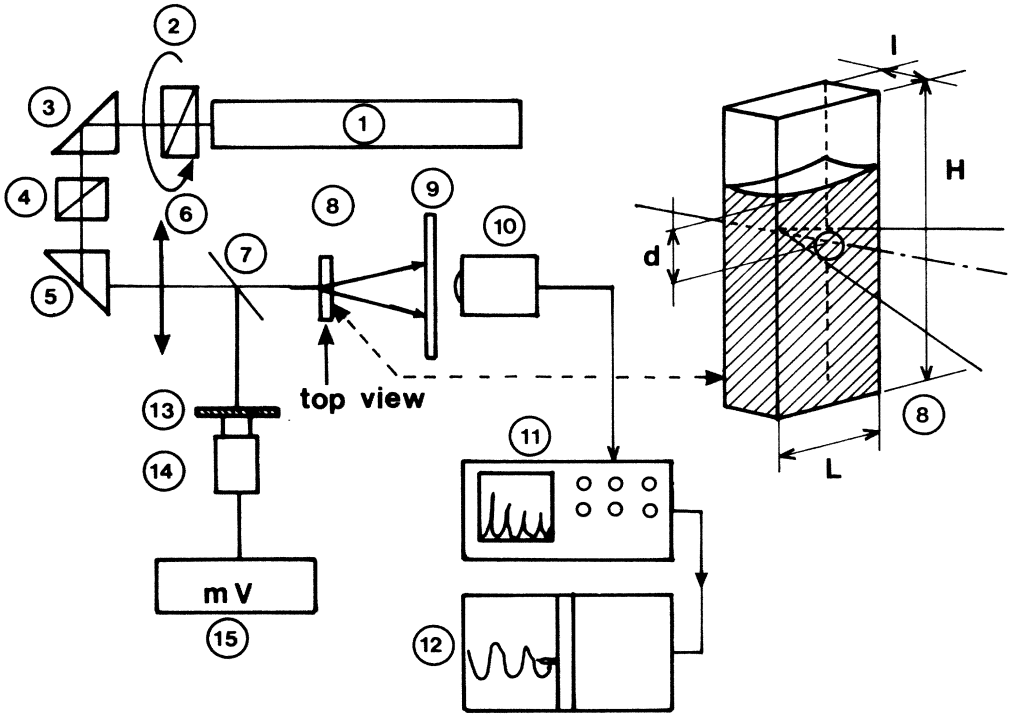

FIG. 1. Experimental setup.

more important, role, which is to smooth out the optical signal collected by the p-i-n photodiode (item 10), with a 1-mm^2 collecting surface, located just behind the screen, and centered on the optical axis. The working area of the photodiode is small with respect to the heartbeat area (typically 4–5 cm^2). In the absence of the screen, the detector would sample a limited portion of the ring pattern. The signal would then contain numerous harmonics linked to the motion of the fringes. We are not interested in the fringe modulation which is essentially an optical interference phenomenon. We are only interested in the global modulation of the pattern which is linked to the hydrodynamic oscillations in the bulk. The presence of the screen enables us to select this global modulation. A spectrum obtained with the presence of the screen is then much simpler than a spectrum obtained without it and reveal actually more essential features.

The photodiode signal is fed to a fast Fourier transform (FFT) spectrum analyzer (item 11) Hewlett-Packard 3582A, which computes and displays the root square of the signal power spectrum. The spectrum, or the signal in the time domain, is then drawn on an X-Y recorder (item 12).

The optical elements 3–10 and 13 and 14 are fixed on a stable optical support. The ambient temperature is controlled within typically 0.5 K for a 3-h experiment.

B. The liquid under study

Numerous liquids have been tested in previous (see references) and present experiments. For the results reported in the present paper, we decided to choose a liquid (and experimental conditions) giving birth to signals as sinusoidal as possible after the first bifurcation from the steady state to the periodic state, producing an amount of harmonics as small as possible.

Figure 2(a) shows a typical signal in the time domain for liquids with high Prandtl numbers (silicon oils, "chromic acid cleaning mixture," for instance), while Fig. 2(b) corresponds to a signal for a liquid pertaining to the class of low Prandtl number liquids (volatile organic solvents such as carbon tetrachloride, toluene, acetone). The signal is not symmetric with respect to the mean value and takes the form of temporal peaks associated with the contraction of the HB, separated by relaxation periods. The two time scales mentioned in Sec. II B appear clearly. They can be defined as the period T of the signal and the peak width at half height δt. For a sinusoidal wave, the ratio $R = 2\delta t / T$ characterizing the

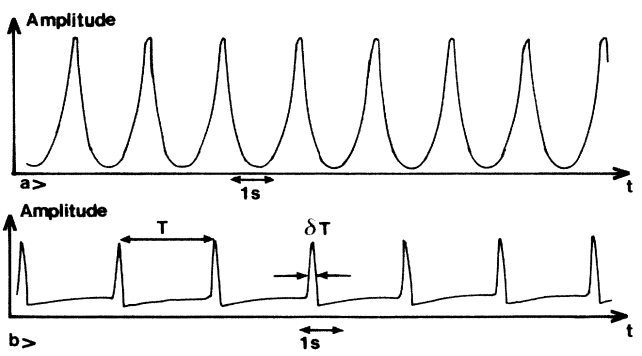

FIG. 2. Two kinds of basic periodic signals in the time domain: (a) silicon oil 47V5, and (b) carbon tetrachloride.

peak steepness is equal to 1. It ranges from 1 to 3 for silicon oils, and from 7.5 to 8.5 for the organic solvents we tested. Consequently, we chose to study a silicon oil. The final choice was the Rhodorsil silicon oil labeled 47V5 which leads to low critical thermal constraint values.[26,27,29] The amount of harmonics also depends on the light collecting system, the chosen one being described in Sec. III A.

IV. QUALITATIVE DESCRIPTION OF THE OBSERVED BIFURCATIONS

A. Generalities

The first bifurcation corresponds to a transition between a steady thermal lens to a periodic one (that we shall call basic), and displays very similar qualitative characters regardless of which liquid is under study. The amplitude of the successive spectral peaks decreases exponentially with the harmonic order, corresponding to a linear decrease in semilogarithmic coordinates (Fig. 3).

A second bifurcation destabilizes the basic periodic state, its properties depending on the liquid under study, and, for a given situation, on the location in the control parameter plane (P,d). The most probable transition is to a two fundamental frequency quasiperiodic state, with the possible occurrence of frequency-locking phenomena, and the existence of a hysteresis zone. We also observe a doubling period transition which is the starting point of a Feingenbaum subharmonic cascade.

In the present work higher-order bifurcations involve other period-doubling transitions. Spectra up to $f_0/16$ (corresponding to five bifurcations from the steady state) were observed, f_0 being the fundamental frequency of the basic periodic state. Transition to chaos is possible,[26,27] although it has not been observed with the present experimental setup.

B. Quasiperiodic states (QP states)

We call primary peaks the ones existing in the basic periodic regime spectra. At the transition to the QP state, four secondary peaks very often emerge simultaneously in each interval between two successive primary peaks (Fig. 4). We found that

$$\delta_1=\delta_2=\delta_4=\delta_5=\delta ,$$

but, in general, δ_3 is not equal to δ. The above δ_i values are the same regardless of the interval $[kf_0,(k+1)f_0]$. The respective amplitudes of the peaks are sketched in Fig. 4. Obviously, the amplitudes in this complete structure decrease when the order k of the interval increases.

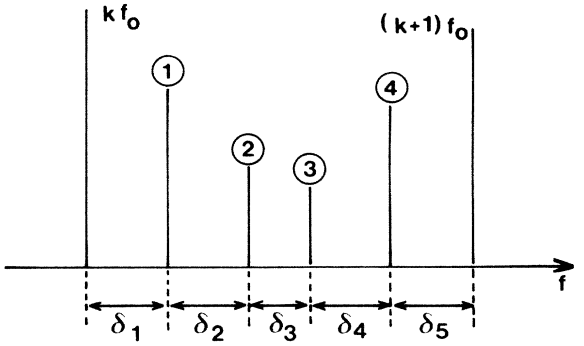

FIG. 4. Sketch showing an example of secondary peak spacing in a bifurcated spectrum.

In other cases, five (instead of four) secondary peaks appear in each interval, with $\delta_1=\delta_2=\delta_3=\delta_5=\delta_6$ different from δ_4, with a similar amplitude structure as in the previous case.

An example of a still more complex and general situation, in which an amplitude hierarchy is not so easy to describe as before, is shown in Fig. 5. A large number of secondary peaks simultaneously emerges between two primary peaks. The exponential decrease of the primary peak amplitudes with respect to the peak order k is preserved. The frequency intervals defined by the secondary peaks between the primary peaks of order k and $(k+1)$ do not depend on k. The amplitude of the peaks varies from 0 (arbitrary value for the fundamental) to -50 dB for the peaks we identify. It is actually expected that a large number of peaks, with still smaller ampli-

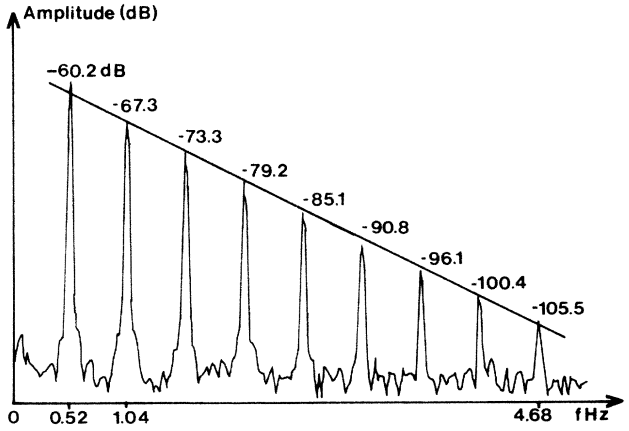

FIG. 3. Basic periodic spectrum, silicon oil 47V5.

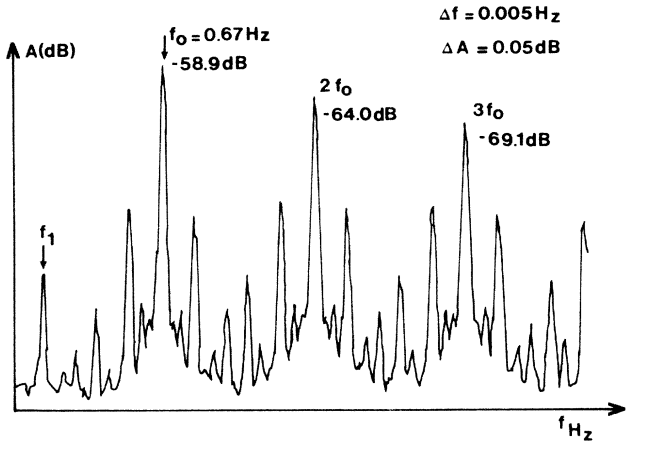

FIG. 5. A bifurcated spectrum, silicon oil 47V5 colored with Red Organol, BX1750, 3 mg/l, $d=1$ mm, $P=200$ mW.

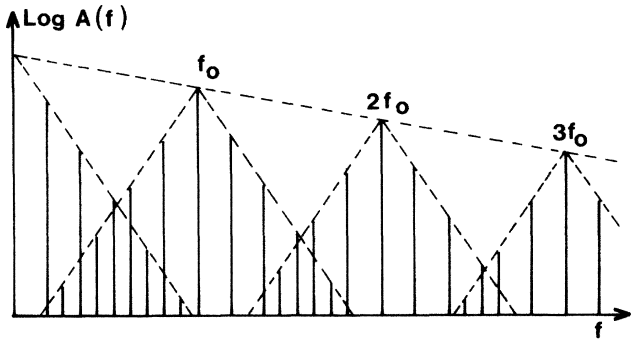

FIG. 6. Sketch of a basic periodic spectrum.

tudes, do exist but are hidden by a nonchaotic background noise. In each interval $[kf_0,(k+1)f_0]$, except the case $k=0$, there is a strong symmetry for the peak location: a peak at (kf_0+f) is associated with a peak at $[(k+1)f_0-f]$ with an equal or nearly equal amplitude.

The spectrum represents a QP state with two fundamental frequencies f_0 and f_1 (chosen, for instance, as shown in Fig. 5). Near the onset of quasiperiodicity, f_1 is equal or nearly equal to $f_0/5$. Then only four secondary peaks emerge between two successive primary peaks (situation sketched in Fig. 4). Interval δ is equal to f_1. Interval δ_3 is equal to the difference between (kf_0+2f_1) and $[(k+1)f_0-2f_1]$, that is to say (f_0-4f_1). δ_3 is nearly equal to f_1 because f_1 is nearly equal to $f_1/5$.

A simplified sketch of the actual spectrum is shown in Fig. 6. We observe the exponential decrease of the primary peak amplitudes when the order k increases. Centered on each primary peak, there is a satellite set of secondary peaks regularly located, with a symmetrical exponential decrease of the amplitudes. The satellite sets interpenetrate to produce the whole spectrum characterized by a double hierarchy of exponential decreases. Furthermore, the absolute values of the decrease slopes in the semilogarithmic scales of Fig. 6 are equal or, at least, nearly equal, irrespective of k.

C. Between quasiperiodicity and the subharmonic cascade

In some cases, by modifying the distance d at a fixed P, we observe a d range where the oscillations are periodic with a fundamental frequency f_0, located between a QP range and another range for subharmonic bifurcations. However, these periodic oscillations do not display the same qualitative features as the ones described previously. The exponential decrease is only asymptotically reached, when the order k of the peak increases, and some peaks of small order $(2f_0,3f_0,4f_0\ldots)$ are characterized by a small amplitude: the signal in the time domain becomes nearly sinusoidal.

D. Subharmonic bifurcations

At high laser powers (about 400 mW), we can observe a transition between the basic periodic state (frequencies $f_0,2f_0\ldots$) and a first subharmonic dynamical state $(f_0/2,f_0,3f_0/2\ldots)$. The control parameter values for this transition are well defined. The amplitude of the secondary subharmonic peaks $(f_0/2,3f_0/2,5f_0/2\ldots)$ increases from 0 when the distance to the onset values increases. The reversible supercritical transitions from the steady state to a basic periodic state, then to a subharmonic periodic state with a fundamental frequency equal to $f_0/2$, form the first steps of a subharmonic cascade.

Higher-order subharmonic bifurcations with fundamental frequencies equal to $f_0/4,\ldots,f_0/16$, were also observed. Examples for $f_0/8$ and $f_0/16$ spectra are shown in Fig. 7. But the onset values are not precisely known due to their strong sensitivity to external conditions, such as the external temperature. Higher-order bifurcations may appear or disappear suddenly, even though the dynamical state prior to the transition was stable for a long period of time. A special study of this cascade would certainly require a more careful temperature control. Some observations for the transition between the $f_0/2$ and $f_0/4$ regimes suggest that it might exhibit (i) hysteresis, and (ii) amplitude discontinuities. If confirmed, this qualitative behavior would significantly differ from the one exhibited by the logistic map. Due to the potential importance of such a difference between the logistic map results and our experimental observations, specific experiments devoted to this problem are planned. However, even now, a departure from the logistic map model does exist, as shown in Fig. 7. In effect, in the logistic map, there is a well-defined hierarchy between

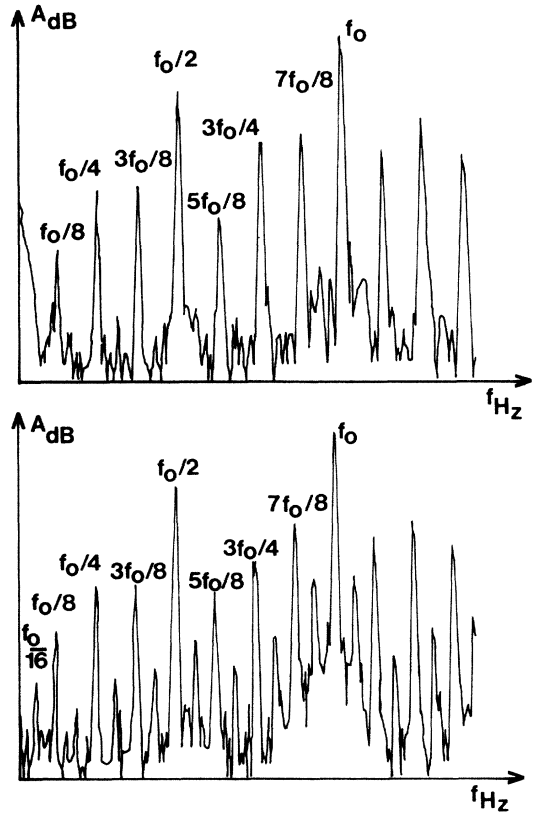

FIG. 7. Examples of highly bifurcated spectra. (a) $f_0/8$ state, $d=0.5$ mm, $P=490$ mW. (b) $f_0/16$ state, $d=0.5$ mm, $P=491$ mW.

the amplitudes appearing in the spectra through successive bifurcations, the newer amplitudes being always smaller than the older ones, in relation with the existence of universal numbers owning some kind of universal character. Conversely, Fig. 7 spectra does not comply with this qualitative rule. For instance, the amplitude of the peak $7f_0/8$ is higher than the amplitude of the peak $3f_0/4$, and the amplitude of the peak $3f_0/8$ is higher or at least not significantly smaller, than the amplitude of the peak $f_0/4$. Admittedly, it is possible to argue that the level of bifurcation is not high enough to approach the universal behavior of the logistic map. However, in the logistic map, the hierarchy between the amplitudes appearing in the spectra through successive bifurcations is qualitatively always observed, even for the first bifurcation steps.

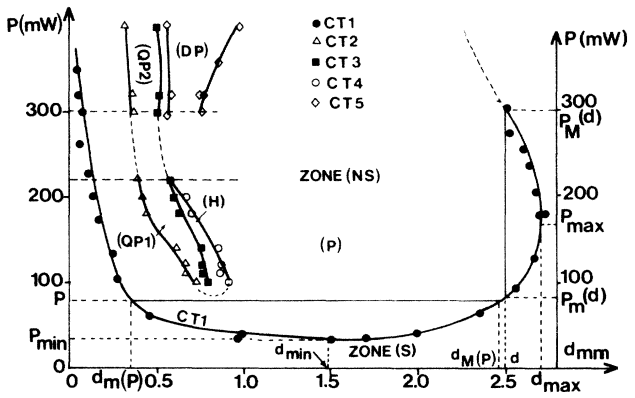

FIG. 8. The different dynamical states in the plane (P,d).

V. IDENTIFICATION OF THE DYNAMICAL STATES IN THE CONTROL PARAMETER PLANE (P,d)

A. Experimental procedure

The rest of the paper is devoted to quantitative experimental results. The experimental procedure is described in this section.

The liquid was a Rhodorsil silicon oil 47V5, colored by a Red Organol BX1750, with a concentration equal to 6 mg/l. The cell dimensions were 5 mm (thickness), 10 mm (lateral width), 45 mm (height). Two series of experiments were carried out. For the first one, the laser power P ranged between typically 300 and 400 mW. The external temperature T_{ext} was controlled between 22.1 and 22.8 °C. For the second series, when P ranged between 30 and 220 mW, the external temperature was controlled between 22.4 and 22.6 °C.

The control parameters were P and d. In more extensive experiments, a third control parameter would be the dye concentration. Observations and measurements have been carried out by scanning d for a fixed P. The experimental procedure has been carefully designed to permit a good control of the experimental conditions. For instance, stabilization of the laser power, external temperature, and adjustment of one distance d, requires about three hours of work.

The reference $d=0$ is obtained by lowering the sealed cell until the appearance on the screen of a vertical luminous line corresponding to the reflection of the laser beam on the meniscus in the cell. This adjustment is carried out for a very small value of the power P to avoid beam divergence. The accuracy on d is estimated to be 0.02 mm. Scanning on d is carried out by steps equal to 0.02 mm, or 0.1 mm, depending on whether interesting phenomena are detected or not.

B. General presentation of the dynamical states and transitions

The parameter plane (P,d) was systematically explored. More than 400 points of the plane were studied.

The following dynamical states were observed: steady, periodic with one basic fundamental frequency, quasiperiodic with two fundamental frequencies, and periodic by period doublings from the basic periodic state.

The following transitions were observed: steady-to-periodic, periodic to quasiperiodic, periodic-to-periodic by period doubling. We must also mention, for P larger than 300 mW, the transition from a quasiperiodic state to a subharmonic periodic state, and the presence of hysteresis at small laser power for a transition periodic-to-quasiperiodic. All these features are now discussed in some details by reference to Fig. 8.

C. The transition steady to unsteady

The steady to unsteady (periodic with one basic fundamental frequency) transition takes place on a curve CT1 in the (P,d) plane, separating an S zone (steady) from a NS zone (nonsteady). The transition is supercritical: the amplitude of the spectrum peaks increases continuously from zero, in a reversible way, when the CT1 is crossed from the S to the NS domain.

There exists a laser power $P_{min}=34$ mW, associated with a distance $d_{min}=1.5$ mm, below which the state is always steady irrespective of distance d. Also, there exists a distance $d_{max}=2.7$ mm, associated with a power P_{max} equal to about 160 mW, above which the state is always steady, for any power P. Furthermore, the existence of a power P above which oscillations do not exist in principle is likely, although that power might be too high to be observable in practice. The zone NS would then be limited by a closed CT1. Such a power does exist in the HB2 case.[26]

For P larger than P_{min}, oscillations exist for d between two values $d_m(P)$ and $d_M(P)$. For d smaller than $d_M(P)$, but not too much smaller, oscillations are observed for P between two values $P_m(d)$ and $P_M(d)$. Furthermore, we can observe a power P equal to about 360 mW for which $d_m(P)$ is zero. It is even possible to observe oscillations for negative d values, a fact which is connected with the existence of a meniscus and with the lateral finite extension of the laser beam.

These quantitative results in the HBE must be put in relation with the ones obtained in the HWE (Sec. II B,

and Refs. 27 and 29). In the HWE the thermal constraint is produced by a temperature difference ΔT, instead of a laser power P. Recent experiments in the HWE (Ref. 34) have shown that there is a linear relation between the difference temperature ΔT and the Joule power dissipated in the hot wire, then fed to the liquid. Consequently, we must expect similar quantitative results between the HWE and the HBE when results are presented using dimensionless forms.

Figure 9 compares $\Delta T_* / \Delta T_*(d_{\min})$ in the HWE and $P_* / P_*(d_{\min})$ in the present experiments, versus $d/d_{\min}$, where the star subscript designates critical quantities for overstability. In the HWE, d is the distance between the hot wire and the free surface, and $d_{\min}$ is equal to approximately 0.9 mm. The comparison (circles and open triangles) shows a striking similarity between the reduced critical profiles for the onset of overstability. There is, however, a significant difference for $d/d_{\min}$ smaller than 1.

This difference is interpreted as being caused by the existence of a meniscus in the HBE and also by the fact that the geometry is confined. The incident laser starts diverging at the entrance point in the cell, near the entrance wall. The thermal plume interacts with this wall and also to some extent with the opposite wall. In the HWE the hot wire is located far away from any wall (nonconfined geometry) and the meniscus has no influence on the phenomena. The height of the meniscus denoted by d_{men} in the HBE is estimated to be $d_{\text{men}}=0.25$ mm. When d and $d_{\min}$ are replaced by $(d+d_{\text{men}})$ and $(d_{\min}+d_{\text{men}})$, respectively, the comparison becomes nearly perfect for $d/d_{\min}$ smaller than 1 (circles and closed triangles), and remains good for $d/d_{\min}$ larger than 1.

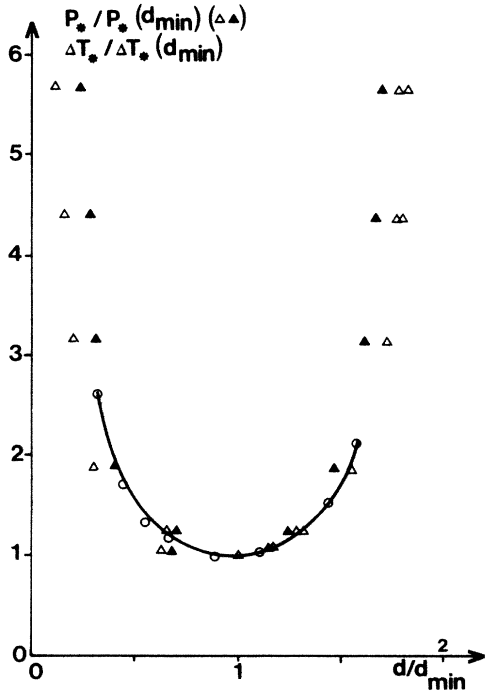

FIG. 9. Reduced profiles for the transition steady to periodic. Comparison between the HBE and the HWE.

D. The transition periodic to quasiperiodic at small laser powers ($P < 220$ mW)

This transition involves the boundaries CT2, CT3, and CT4 in the parameter plane (Fig. 8) and leads to the existence of the domains QP1 (QP states with two fundamental frequencies) and H (hysteresis). The boundary CT2 corresponds to a supercritical transition (continuity and reversibility) while zone H is reached via a subcritical transition (discontinuities and irreversibilities associated with hysteresis phenomena). In zone H two states are possible, the one actually observed depending on whether the experiments are carried out by increasing or decreasing d. The total width of the domain QP1 plus H is never greater than about 0.27 mm; that is an order of magnitude smaller than zone NS. Frontiers CT2 and CT4 have been joined by a dashed line which actually does not correspond to experiments but to a conjecture. This line corresponds to a domain in which periodic states are actually observed, but in which QP states are potentially present. This domain would require a specific study, for instance, by working at a fixed d and modifying P, to attempt to reveal the potential quasiperiodic states. Unfortunately, a P scanning is much more difficult to control than a d scanning.

Details of this transition are explained using Fig. 10. We choose a laser power P crossing zones QP1 and H. In a first d scanning, we decrease d starting from a very large d [Fig. 10(a)]. The state is steady S. At $d=d_M(P)$, the state becomes periodic with one fundamental frequen-

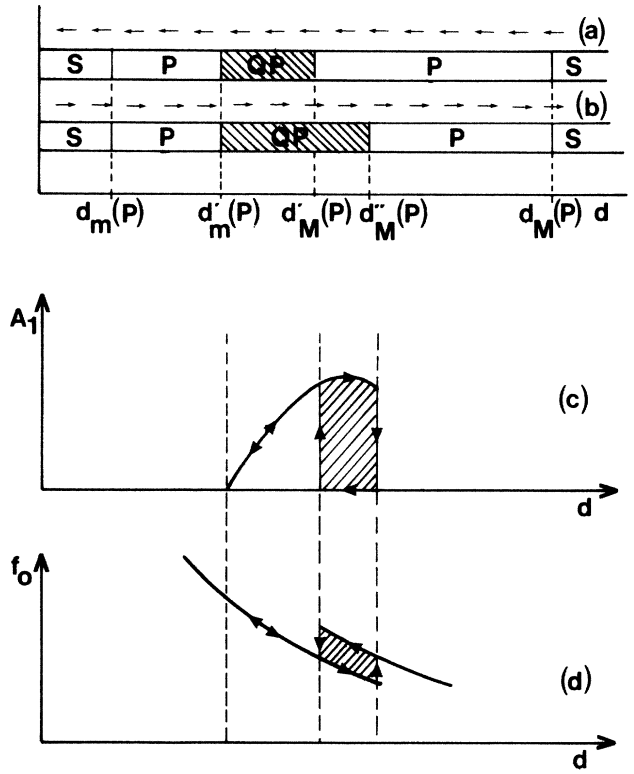

FIG. 10. Qualitative characterization for the transition periodic to quasiperiodic.

cy f_0 (zone P). The associated amplitude A_0 is equal to zero at the transition S-P and increases when d decreases, while f_0 increases. At $d=d'_M(P)$, where we cross CT3, a subcritical bifurcation leads to a QP state with two fundamental frequencies. The amplitude A_k of any secondary peak undergoes a discontinuous modification, from 0 to a finite value [Fig. 10(c)], accompanied by a frequency jump for f_0 to a lower value [Fig. 10(d)]. When d decreases again, the amplitude A_k (say, A_1) decreases continuously, down to 0 at $d=d'_m(P)$, where the system undergoes a supercritical transition to the basic periodic state. Finally, the steady state is recovered at $d=d_m(P)$. Increasing d from zero [Fig. 10(b)] we then obtain a transition sequence of the kind S-P-QP-P-S. However, the subcritical transition QP-P appears at $d=d''_M(P)$ instead of $d=d'_M(P)$, showing an hysteresis domain H in the range $[d'_M(P)/d''_M(P)]$.

E. Period-doubling transitions

Period-doubling (DP) transitions can be observed in zone DP (Fig. 8). The first period-doubling transition (emergence of secondary peaks at $f_0/2, 3f_0/2, \ldots$) is supercritical and takes place on line CT5. Period-doubling states of the kind $f_0/4, f_0/8, f_0/16$, were also observed inside domain DP but the extension of the corresponding domains is comparable to experimental inaccuracies, preventing us from defining boundary locations. Also, the system can jump spontaneously from a $f_0/8$ state to a $f_0/16$ state (for instance), due probably to sensitivity to external conditions.

F. The quasiperiodic states at high laser powers ($P > 300$ mW)

A two-fundamental-frequency QP domain QP2, limited by lines CT2 and CT3, is observed at high laser powers ($P > 300$ mW). Zones QP1 and QP2 are probably connected as indicated by the dashed lines. The P-QP transition is supercritical on CT2. The relation between domains QP2 and DP requires a more special discussion.

G. The relations between domains QP2 and DP

When power P increases, the width of QP2 is almost constant while the width of DP increases. Consequently, the relative importance of the period-doubling phenomena increases with the laser power. Domains QP2 and DP are close, but remain distinct. The nature of the states between these two domains is not always easy to determine. The subcritical transition leading to QP1, for a fixed P, and d decreasing, starts from the basic periodic state. Conversely, the subcritical transition leading to QP2, for a fixed P, and d decreasing, starts from a period-doubled state of the $f_0/2$ type.

Details are explained in Fig. 11. For a fixed $P > 300$ mW, we start from a point located in zone S and decrease d. Basic periodic oscillations (zone P) appear at $d_M(P)$. Then we enter a DP zone (period doubling leading to $f_0/2$ states) through a reversible supercritical bifurcation. A black domain of very small width indicates the existence of higher-order period-doubled states. With distance d decreasing again, subharmonic states of the kind $f_0/2$ are recovered. A second black domain of small width indicates the junction between domain DP (DP states) and QP2 (QP states). Two kinds of behavior have been observed in this junction domain. In most cases, we recover the basic periodic state with fundamental frequency f_0 prior to the onset of quasiperiodicity. In other cases, the QP states emerge directly from the subharmonic $f_0/2$ states. In the latter case, the distinction between QP and $f_0/2$ states is somewhat artificial because the $f_0/2$ states can be understood as a two fundamental frequency QP state with frequency locking $f_0/f_1=2$. The transition to quasiperiodicity must then be understood as an unlocking followed by a continuous change of the ratio f_0/f_1 as d goes on decreasing. The two above variants were for instance observed under the same conditions, except for a small difference equal to 0.6 °C for the external temperature which is probably not sufficient to explain the difference of behaviors because, in other cases, such a difference did not modify the nature of the transition to the QP states. Other noncontrolled experimental details must intervene, such as the delay between two modifications of distance d for instance.

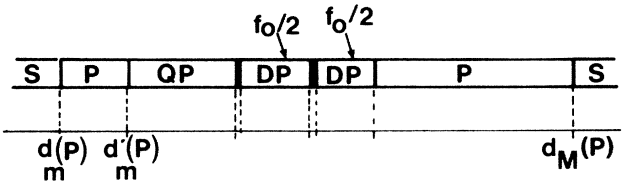

FIG. 11. Qualitative characterization for the transition between quasiperiodicity and subharmonic cascade.

Finally, if we continue to decrease d, we observe the QP-P transition at $d=d'_m(P)$ followed by the P-S transition at $d=d_m(P)$. If d is now increased, the same sequence of transitions is observed in the reverse way, without any hysteresis.

VI. SPECTRAL ANALYSIS OF THE UNSTEADY STATES

A. Frequencies and amplitudes: Definitions

For the basic periodic states, f_0 is the fundamental frequency. For the QP states (zones QP1 and QP2), f_0 is defined by continuity from the basic periodic state. This definition shows no ambiguity because it is always possible to go from a periodic state P through a QP state via a supercritical transition. It happens that, for these states, f_0 is also the frequency of the highest peak. For the period-doubled states, f_0 is again defined by continuity from the basic periodic state. However, f_0 is no longer the fundamental frequency for these states. Furthermore, for these states, the subharmonic peak $f_0/2$ may be higher than the fundamental peak, in contrast with the logistic map behavior.

A_0 is the amplitude of the peak of frequency f_0. Comparison between different A_0 values only makes easy sense for a fixed P, and various d. When P is modified, the relation between A_0 and the hydrodynamic state in the cell becomes complicated because it integrates several effects: the modification of the state induced by the power modification, but spoiled by the fact that the divergence of the laser beam is also modified by a pure thermal lens effect. Consequently, the dependence of A_0 on P will not be discussed.

B. Dependence of f_0 and A_0 on distance d

Figure 12 shows the values of frequency f_0 versus d, for selected values of P. A_0 values are given in Fig. 13. The functions $f_0(d)$ and $A_0(d)$ are defined for d ranging in zone NS, between $d_m(P)$ and $d_M(P)$.

All the amplitude profiles are similar. They contain three different parts labeled A,B,C in Fig. 13 for $P=320$ mW. Part A is located near the onset value $d_m(P)$. The amplitude increases very fast from -90 dB (experimental noise), up to -40 dB, for a small change of d, equal to 0.1 mm at $P=34$ mW and to 0.2 mm at $P=300$ or 400 mW. In part B, the amplitude decreases when d increases. The decrease is approximately exponential, corresponding to a linear decrease in Fig. 13 (amplitudes expressed in dB). In the zone at the boundary between A and B, the amplitudes randomly vary by a factor of 2 depending on the experiments. In part C the decrease slope becomes larger as we approach $d_M(P)$. Eventually, the amplitude changes from -50 to -80 dB, for a change of d equal to about 0.1 mm.

The variation of frequency f_0 with respect to d can be well fitted by an hyperbolic decrease, modified in three parts labeled D,E,F (Fig. 12). Part D, near $d_m(P)$, corresponds to frequencies smaller than the basic hyperbole values. Frequencies fluctuate from one experiment to the next but are nearly constant with respect to d when they are averaged. The region labeled E corresponds to the hysteresis (zone H in the parameter plane). Finally, in part F, frequencies increase slightly above the hyperbolic profile when d approaches $d_M(P)$.

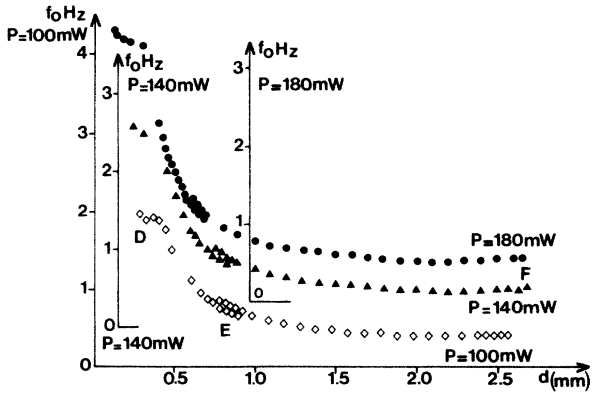

FIG. 12. Fundamental frequency f_0 vs distance d for $P=100$, 140, and 180 mW.

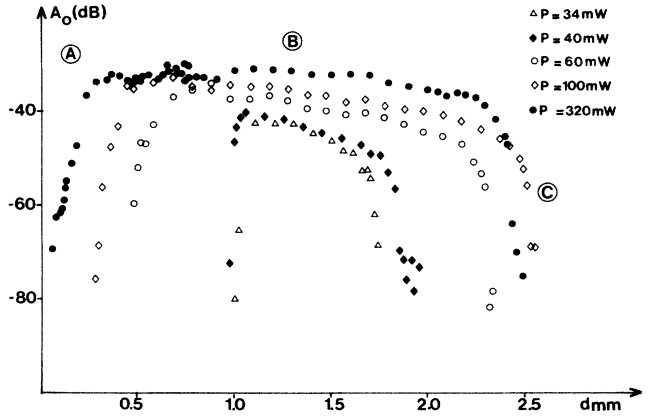

FIG. 13. Amplitude A_0 of the fundamental peak vs distance d for various P values.

C. Dependence of f_0 on power P

Frequency f_0 is shown versus P for various d values in Fig. 14. For a given d, the profile shows a steep linear increase at small P followed, after a slope-breaking range, by another linear increase, although with a small slope. At large d values, only the small slope increase is observed, while, for $d=0.15$ mm, we only observe the steep increase behavior. The slopes for the small slope ranges do not significantly depend on d, within experimental uncertainties, and the values of the frequencies increase when d decreases. Furthermore, for any d, the points in the steep slope range collapse on a single curve. Comparing with Fig. 8, we see that slope breakings are observed when we approach values $d_m(P)$.

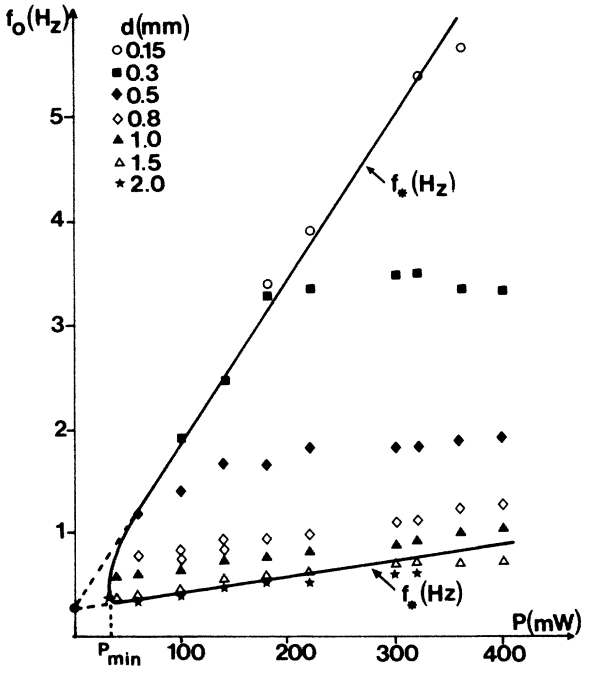

FIG. 14. Fundamental frequency f_0 vs power P for various values of the distance d. The critical frequencies for marginal overstability f_* are also indicated.

D. The onset frequency for the S-P transition

The critical frequency values f_* for the onset of overstability (CT1) are given as $(f_* d)$ versus d in Fig. 15. For d smaller than $d_{\min}$, the f_* profile is hyperbolic (label B), except for d smaller than 0.15 mm. In this last zone, labeled A, near the free surface, f_* increases less than $1/d$ when d decreases. Experimental uncertainties become very great. For d smaller than 2.26 mm, there is a single onset frequency for a given d value. For d ranging between 2.26 and 2.73 mm ($d_{\max}$, Fig. 8), in the zone labeled C corresponding to the right branch of the CT1 (Fig. 8), two frequency values are associated with a given d value. They are $f_*[P_m(d)]$ and $f_*[P_M(d)]$, the former being smaller than the latter. At $d = d_{\max}$, these two frequencies collapse to a single value.

The onset frequencies f_* are also reported in Fig. 14. Two onset frequencies are associated with each P value (compare with Fig. 8), corresponding to distances $d_{\min}(P)$ and $d_{\max}(P)$, the value for $d_{\min}(P)$ being greater than the one for $d_{\max}(P)$. We observe that the steep slope parts of the profiles in Fig. 14 coincide with the onset frequency for $d_{\min}(P)$. The upper and lower branches of the profile $f_*(P)$ are joined at $P = P_{\min}$. When the linear part of each branch is extrapolated to $P = 0$ (Fig. 14, dashed lines), they define a single frequency $f_*(P = 0)$. The loss of linearity of the upper branch is located between $P = 60$ mW and $P = P_{\min}$. Near the junction point at $P = P_{\min}$, the upper branch tends to become parallel to the vertical axis. The derivative of f_* with respect to P becomes very great, or even infinite. The value $P = 60$ mW also corresponds to a great modification of the slope in the left branch of the CT1 (see Fig. 8).

In Sec. V C, the critical thermal driving constraints in the HBE and in the HWE were compared. Similarly, critical frequencies for the onset of overstability between both kinds of experiments are compared in Fig. 16 using reduced values $f_*/f_*(d_{\min})$ versus $d/d_{\min}$. The profiles are very similar. However, critical frequencies in the HBE are much smaller than in the HWE for $d/d_{\min}$ smaller than 1. A first correction for the HBE is carried out by replacing d by $(d + d_{\text{men}})$ and $d_{\min}$ by

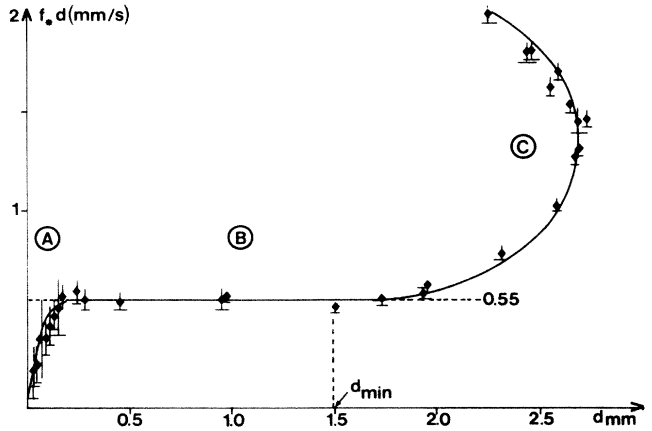

FIG. 15. The product $f_* d$ vs distance d.

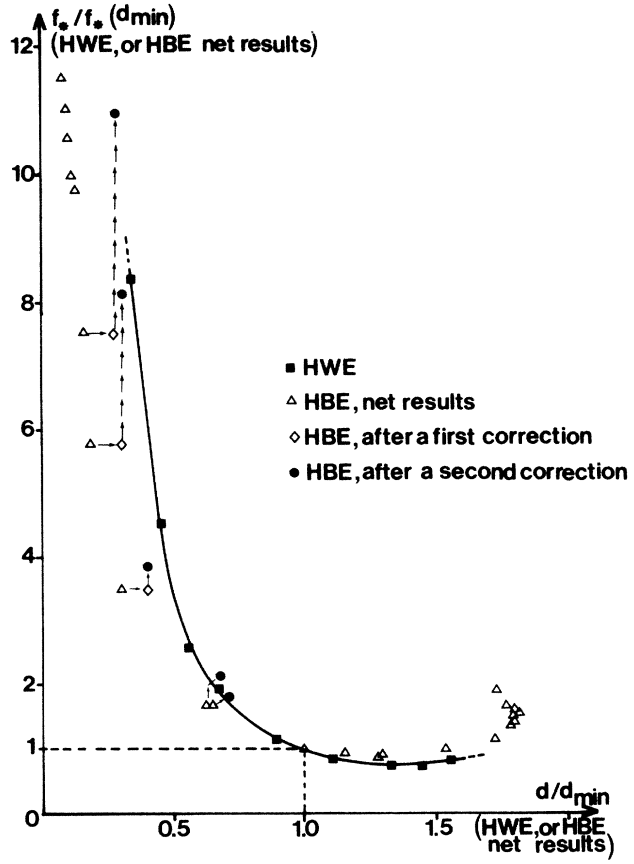

FIG. 16. Reduced profiles for critical frequencies f_*. Comparison between the HBE and the HWE.

$(d_{\min} + d_{\text{men}})$, as done in Sec. V C. Although this correction leads to closer profiles, it is still insufficient.

A second correction is now carried out as follows. To the purpose, we observe that, in the HWE, the fundamental frequency of the oscillations f_0 varies as $1/d$, ΔT being fixed, when d is scanned on the whole range where oscillations do exist.[34] In the HBE this hyperbolic profile is not valid when d approaches the onset value $d_m(P)$, as seen, for instance, in Fig. 12 in the zone labeled D. The difference between reduced frequency profiles in Fig. 16 is attributed to the difference of above-mentioned behaviors between the HBE and the HWE when d approaches $d_m(P)$. The resulting correction has been carried out, for each value of P, by replacing the frequency $f_*[P, d_m(P)]$ by the value $f_0[P, d_m(P)]$ that we would observe in the HBE if the hyperbolic profile were valid up to $d = d_m(P)$. After this second correction, there is a very good agreement in Fig. 16 between the reduced frequency profiles for the HBE and HWE.

E. The onset frequencies for the P-QP transition

For this transition, five onset frequencies must be defined for each P value, due to hysteresis. One onset frequency corresponds to $d = d'_m(P)$. Furthermore, two onset frequencies are associated with $d = d'_M(P)$ and two

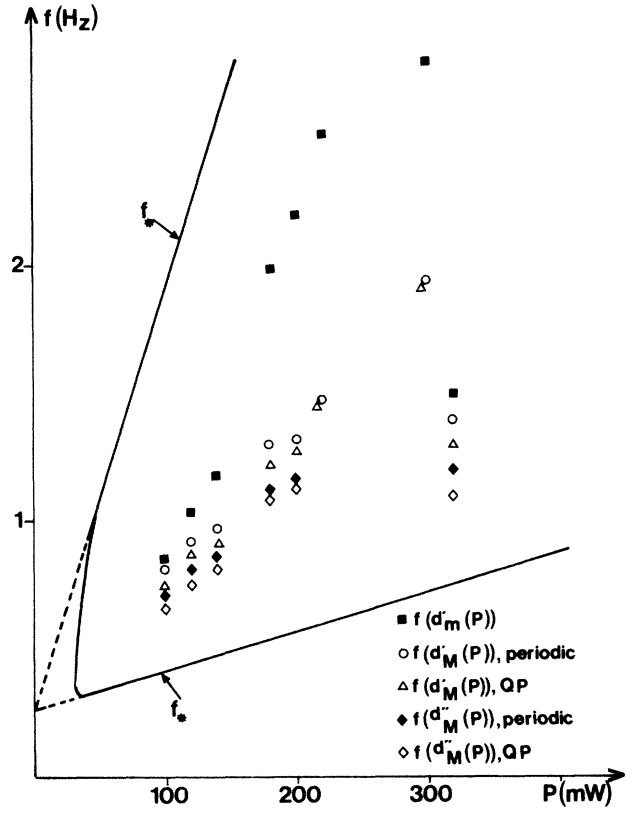

FIG. 17. Fundamental frequencies for the transition between periodicity and quasiperiodicity.

others with $d=d''_M(P)$, as shown in Fig. 10(d). There is no discontinuity in frequency f_0 at the onset distance $d=d'_m(P)$. The onset frequencies at $d=d'_M(P)$ and $d=d''_M(P)$ are larger in the periodic state than in the QP state.

The onset frequencies for the P-QP transition are shown in Fig. 17 in which the onset frequencies f_* are also reported for the sake of comparison. All the onset frequencies P-QP increase when P increases. The frequency jumps at the boundaries of the H zone decrease when P increases from 100 to 200 mW. The difference between the onset frequencies f_* and the onset frequencies for the P-QP transition increases when power P increases.

F. Frequencies in quasiperiodic spectra

Figures 18–20 show the evolution of the frequencies in the QP spectra versus d, for various values of the power P. We limited ourselves to frequencies in the range $(0,f_0)$, from which we can deduce the frequencies in any range $[nf_0,(n+1)f_0]$ by a nf_0 translation along the frequency axis. Only the distances in the range $[d'_m(P),d''_M(P)]$ (see Fig. 10) are discussed, the rest of the oscillation domain being previously discussed in Fig. 12. Frequency lockings (when the ratio f_1/f_0 is rational) are indicated by vertical bands which, when they are narrow

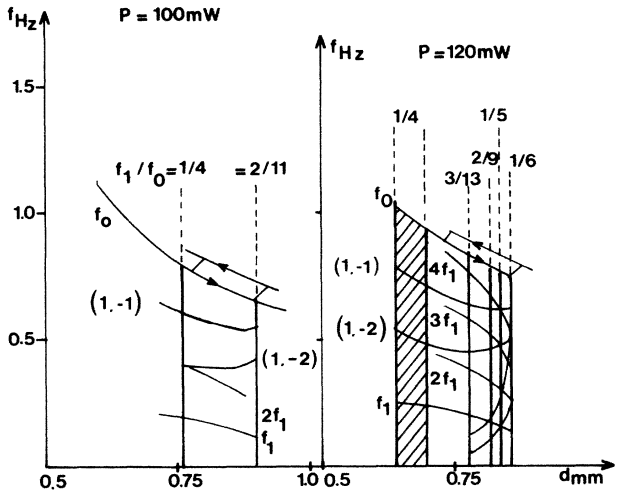

FIG. 18. Oscillation frequencies in the QP state vs distance d, $P=100$ and 120 mW. A frequency of the form (af_0+bf_1) is designated in Figs. 18–20 as (a,b).

enough, collapse to vertical lines.

All the QP frequencies can be formed as a combination of two fundamental frequencies f_0 and f_1. Both the values of f_0 and f_1 increase when d decreases for a fixed P. However, we observe that f_1 is approximately constant when P is modified, for a fixed d. Each curve in Figs. 18–20 is labeled by explicitly designating the corresponding combination law. For instance, in Fig. 18, the curve labeled (1,-2) corresponds to a frequency f equal to (f_0-2f_1). More generally, we call curve index (k_0,k_1) the curve corresponding to a frequency f equal to $(k_0f_0+k_1f_1)$. In certain cases, two or several different

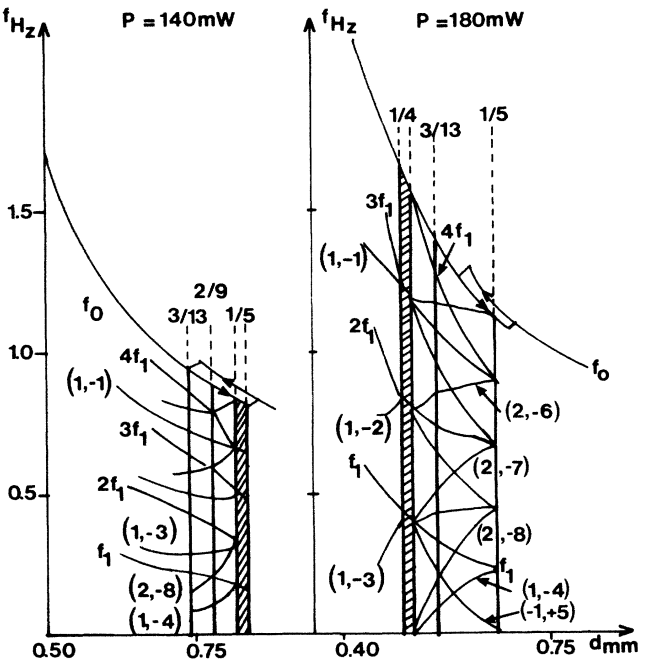

FIG. 19. Oscillation frequencies in the QP state vs distance, d, $P=140$ and 180 mW.

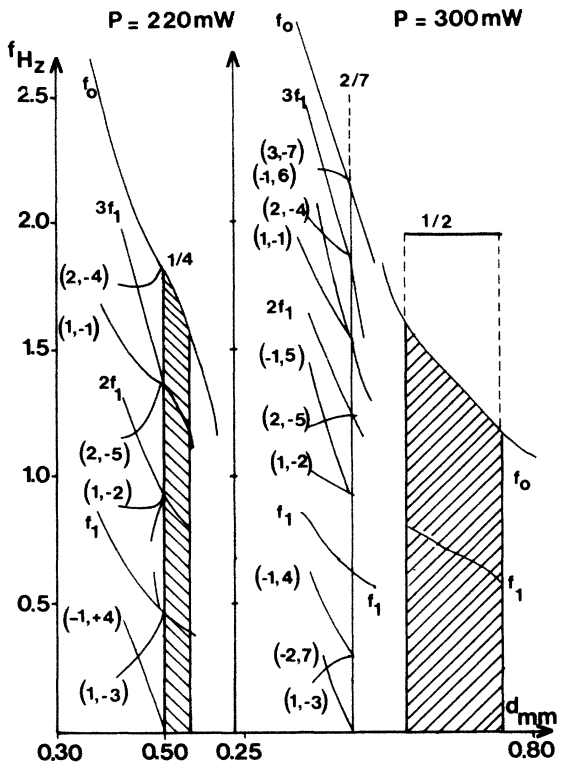

FIG. 20. Oscillation frequencies in the QP state vs distance d, $P=220$ and 300 mW.

curves indexes meet, indicating frequency lockings, producing a decrease of the number of peaks in the spectrum.

Identification of frequency lockings by the above visual criterion has been supplemented by direct computations of the f_1/f_0 ratio which becomes a rational number at frequency lockings (periodic states), while irrational ratios correspond to true QP states. However, this theoretical frequency-locking criterion is not easy to apply in practice due to the limited accuracy of the frequency measurements. It is actually impossible to know whether the ratio of two measured real values is or is not a rational number. In fact, we only used the above determination of the frequency ratio to confirm (from frequency measurements and accounting for the frequency uncertainties) that such frequency locking which was visually detected from the figures was compatible with a rational value for the f_1/f_0 ratio. From a visual observation of the figures, completed by a computational checking of the rational character of the f_1/f_0 ratio, we identified the following f_1/f_0 frequency-lockings states: 1/2, 1/3, 1/4, 1/5, 1/6, 2/7, 2/9, 3/10, 2/11, 3/13, 4/13, 8/17, arranged by increasing values of the denominators. The extreme ratio values are $1/6=0.1666\ldots$, and 1/2 (period doubling).

G. The devil's staircase

The f_1/f_0 ratios versus d, for selected values of P, are shown in Figs. 21 and 22. The uncertainties, essential for the computational confirmation of frequency lockings,

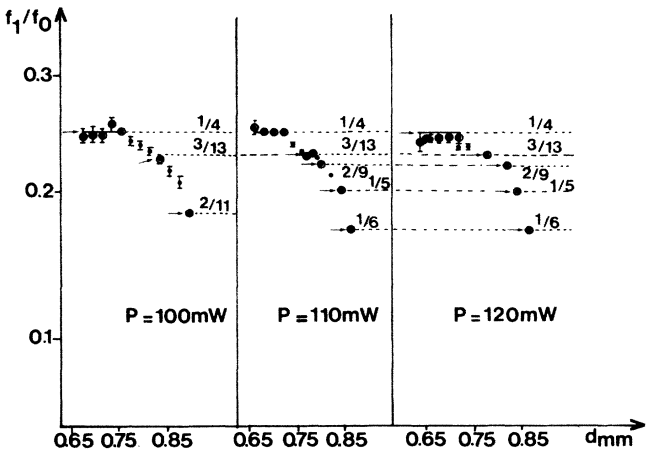

FIG. 21. The ratio f_1/f_0 in the QP state vs distance d for $P=100$, 110, and 120 mW.

are indicated in the figures by a vertical line when this line is high enough to be visible. Identified frequency-locking points are surrounded by a small circle and pointed to by an arrow. The value of the frequency-locking ratios f_1/f_0 are also indicated. Furthermore, the identified frequency-locking ratios are 1/4, 3/13, 2/9, 1/5 at $P=140$ mW, 3/10, 2/7, 1/4, 3/13, 1/5 at $P=180$ mW, 4/13, 3/10, 1/4, 3/13, 2/9 at $P=200$ mW, and 3/10, 1/4 at $P=220$ mW (figures not given).

For P smaller than 300 mW, where periodic-doubling states are not observed, the f_1/f_0 ratios increase when d decreases, and there is a progressive shifting of the curves toward smaller d when P increases (Fig. 21). For P equal to or larger than 300 mW (Fig. 22), QP and period-doubled states are possible. We observe two different curves in each figure, one for the quasiperiodicity (with an evolution of the f_1/f_0 ratio not so clear as in Fig. 21) and the other, a straight line at $f_1/f_0=\frac{1}{2}$, for the first period doubling. In Fig. 22, for $P=400$ mW, we observe a clue for a transition between the QP curve and the period-doubled line. However, a true junction is never obtained because we actually observe a return to the basic periodic state between period doubling and quasiperiodicity.

Theoretically, in a two fundamental frequency QP state, the ratio f_1/f_0 can evolve continuously when a control parameter is modified, but remains constant on

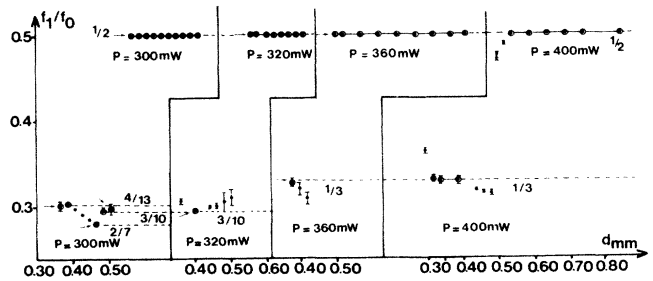

FIG. 22. The ratio f_1/f_0 in the QP state vs distance d for $P=300$, 320, 360, and 400 mW.

intervals when it becomes a rational number p/q. In practice, only some bands corresponding to simple rational numbers can be observed. The finite bands we actually observed correspond to ratios 1/2, 1/4, 1/5. The evolution of the f_1/f_0 ratio forms a curve, called the devil's staircase, which is continuous and remains constant on rational number bands. This curve is sometimes qualified as being fractal. Experimental devil's staircases are suggested by Figs. 21 and 22.

VII. CONCLUSION

The present paper was devoted to the study of dynamical states and transitions observed when thermal-lens oscillations are produced by laser heating an absorbing liquid near and below the free surface. The control parameters are the laser power P and the distance d between the laser and the free surface. The following dynamical states have been identified: steady, periodic with period-doubling bifurcations, and quasiperiodic states with hysteresis phenomena. The transitions have been extensively investigated and discussed. Experimental devil's staircases are presented. The large amount of results given in this paper shows that thermal-lens oscillations provide a system exhibiting very noteworthy behaviors, relevant to the current study of the transition from a steady to a chaotic state.

ACKNOWLEDGMENTS

Laboratoire d'Energétique des Systèmes et Procédés is Unité No. 230 associée au Centre National de la Recherche Scientifique (France).

[1]J. P. Eckmann, Rev. Mod. Phys. **53**, 643 (1981).
[2]P. Cvitanovic, Acta Phys. Pol. A **65**, 203 (1984).
[3]P. Bergé, Y. Pomeau, and C. Vidal, L'Ordre dans le Chaos (Hermann, France, 1984).
[4]D. Ruelle and F. Takens, Commun. Math. Phys. **20**, 167 (1971).
[5]S. Newhouse, D. Ruelle, and F. Takens, Commun. Math. Phys. **64**, 35 (1978).
[6]M. J. Feigenbaum, J. Stat. Phys. **19**, 25 (1978).
[7]M. J. Feigenbaum, J. Stat. Phys. **21**, 669 (1979).
[8]M. J. Feigenbaum, Commun. Math. Phys. **77**, 65 (1980).
[9]P. Manneville and Y. Pomeau, Phys. Lett. **75A**, 1 (1979).
[10]P. Manneville, J. Phys. **41**, 1235 (1980).
[11]P. Manneville and Y. Pomeau, Physica **1D**, 219 (1980).
[12]J. Maurer and A. Libchaber, J. Phys. Lett. **40**, L419 (1979).
[13]S. Rajagopalan and R. A. Antonia, Phys. Fluids, **23**, 1938 (1980).
[14]J. P. Gollub and S. V. Benson, J. Fluid Mech. **100**, 449 (1980).
[15]P. S. Linsay, Phys. Rev. Lett. **47**, 1349 (1981).
[16]R. R. Snapp, H. J. Carmichael, and W. C. Schieve, Opt. Commun. **40**, 68 (1981).
[17]V. Croquette and C. Poitou, J. Phys. Lett. **42**, L537 (1981).
[18]R. Anthore, P. Flament, G. Gouesbet, M. Rhazi, and M. E. Weill, Appl. Opt. **21**, 2 (1982).
[19]J. P. Gordon, R. C. C. Leite, R. S. Moore, S. P. Porto, and J. R. Whinnery, J. Appl. Phys. **36**, 3 (1965).
[20]J. R. Whinnery, D. T. Miller, and F. Dabby, IEEE J. Quantum Electron **QE-3**, 382 (1967).
[21]F. G. Gebhardt and D. C. Smith, IEEE J. Quantum Electron **QE-7**, 63 (1971).
[22]P. M. Livingston, Appl. Opt. **10**, 426 (1971).
[23]C. A. Carter and J. M. Harris, Appl. Opt. **23**, 476 (1984).
[24]H. Sontag and A. C. Tam, Opt. Lett. **10**, 436 (1985).
[25]L. K. Forbes, J. Appl. Math. Phys. **36**, 275 (1985).
[26]G. Gouesbet, M. Rhazi, and M. E. Weill, Appl. Opt. **22**, 2038 (1983).
[27]G. Gouesbet, M. E. Weill, and E. Lefort, AIAA J. **24**, 1324 (1986).
[28]M. E. Weill, M. Rhazi, and G. Gouesbet, C. R. Acad. Sci. (Paris) **294**, 567 (1982).
[29]M. E. Weill, M. Rhazi, and G. Gouesbet, J. Phys. **46**, 1501 (1985).
[30]G. Gouesbet, Phys. Chem. Hydrodynamics **8**, 349 (1987).
[31]J. Maquet, G. Gouesbet, and A. Berlemont, *Numerical Methods in Thermal Problems, Proceedings of the Fifth International Conference on Numerical methods for Thermal Problems, Montréal, 1987,* edited by R. W. Lewis, K. Morgan, and W. G. Habashi (Pineridge Press, Swansea, United Kingdom, 1987), Vol. 5, pt. 1, pp. 472–483.
[32]G. Gouesbet and J. Maquet, AIAA J. Thermophys. Heat Transf. (to be published).
[33]G. Gouesbet and J. Maquet (unpublished).
[34]C. Roze (private communication).